Nineteenth Australasian Wind Engineering Society Workshop, April 4-6, 2018, Torquay, Victoria

Numerical Simulation of Wind-Driven Rain in the Australasian Built Environment using an Eulerian Multiphase Model

Richard Jones[1], Neil Mackenzie[2], Tom Moyle[3]

[1]*Aurecon Group, 55 Grenfell St Adelaide 5000, Australia, Richard.Jones2@aurecongroup.com*

[2]*Aurecon Group, 55 Grenfell St Adelaide 5000, Australia, Neil.Mackenzie@aurecongroup.com*

[3]*Aurecon Group, 55 Grenfell St Adelaide 5000, Australia, Tom.Moyle@aurecongroup.com*

ABSTRACT

Provision of shelter and comfort is fundamental to design of the built environment. While increasingly complex models of environmental conditions are being included in the commercial design process, often Wind-Driven Rain (WDR) intrusion into occupied spaces remains a key complaint particularly for public buildings such as transport terminals and sports stadia. This paper outlines a computational procedure for WDR intrusion modelling based on the Eulerian multiphase method. Specifically, the WDR Eulerian multiphase method is reviewed, key model parameters are discussed and the associated statistical analysis of historical meteorological data is included.

1. Introduction

Numerical modelling of Wind-Driven Rain (WDR) has generally been based on the Lagrangian particle (LP) tracking method originally proposed by Choi (1993). Several extensions to this approach have been suggested, as summarized by Blocken and Carmeliet (2004). These approaches consist of (a) steady-state wind-flow using 3D RANS and turbulent model; (b) injection of one way coupled LP for discrete drop diameters; (c) Calculation of raindrop trajectories; (d) iteratively analyze raindrop trajectories to get Specific Catch Ratios (SCR); (e) calculate the Global Catch Ratio (GCR) from SCR and horizontal raindrop size distribution. The catch ratio is analogous to a percentage of horizontal rainfall intensity and similar to the Driving Rain Index discussed by Lawson (2001). Numerically calculating catch ratios is particularly troublesome using LP tracking, where the droplets that impinge on the edges of a given area must be tracked back to their initial horizontal area and the area ratio calculated (refer Figure 1) for each surface of interest and weather condition.

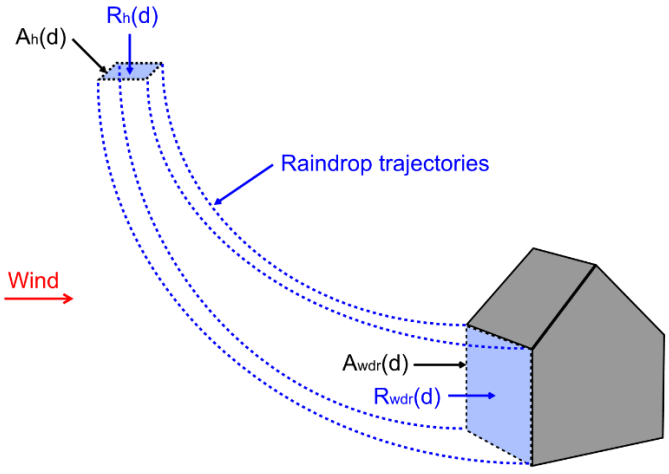

Figure 1: Stream tube bounded by raindrop trajectories

In multiphase flow a phase represents a continuous field of material with similar inertial response to and interaction with the primary flow field. While LP tracking is analogous to raindrop motion, the concept of multiphase flow for rain motion requires explanation. Here a series of continuous fields are created corresponding to a pre-defined raindrop diameter. The phase volume fraction (α_k) represents the density of raindrops of a given diameter (k) in each control volume and the phase velocity field ($\boldsymbol{u}_{r_k}$) represents the velocity of those raindrops. Mass and momentum equations can therefore be defined where gravitational and drag momentum source terms are specified for the given drop diameter. This approach is considerably easier to implement than LP tracking, particularly since SCR and GCR can be directly calculated from field values for complex geometry, making it a viable commercial design tool.

In pursuit of a commercial design tool the current paper is based on the multiphase Euler method of Kubilay et. al. (2013, 2015) briefly outlined in Section 4. However, where previous authors have focused on accurate recreation of WDR for a given rain event, the current paper focuses on environmental conditions (Section 3) and post-processing (Section 4) that yield rain intrusion contours that can be easily understood by building designers and stakeholders. Given that building design is often discussed under typical and worst-case environmental conditions, these descriptions are reflected in the statistical definitions and subsequent simulations.

2. Raindrop Physics

Raindrops and their motion are characterized by rainfall intensity, size distribution and aerodynamic drag. Rainfall intensity, discussed further in Section 3, usually refers to rainfall measured through a horizontal orifice and is expressed millimeters (of height per unit area) per hour.

Rain consists of a spectrum of raindrop diameters. Several empirical studies of raindrop diameter distribution were undertaken in the mid-20th century. Best (1950) conducted a literature survey and numerous on-site measurements and remains an authoritative reference on raindrop size distribution. A graph of raindrop probability density based on Best (1950) is provided in Figure 2.

Aerodynamic drag is a function of shape, frontal area, surface roughness and velocity. At lower velocities a raindrop can retain a smooth spherical shape due to surface tension of the droplet; however, as the raindrop approaches terminal velocity it is deformed by aerodynamic forces, altering the drag coefficient. Droplet drag coefficients were studied by Gunn & Kinzer (1949) and are shown in Figure 2 as a function of droplet Reynolds number (Re_r) defined as

$$Re_r = \frac{\rho_a d}{\mu_a} |\boldsymbol{u}_a - \boldsymbol{u}_r| \tag{1}$$

where d is drop diameter, ρ_a is density, μ_a is air viscosity, $\boldsymbol{u}_r$ is drop velocity and $\boldsymbol{u}_a$ is the air velocity. Any falling object will reach terminal velocity when the gravitational force balances with aerodynamic drag force. The associated water droplet terminal velocities from Gunn & Kinzer (1949) are also included in Figure 2 below. Further information on raindrop physics is provided by Lawson (2001) together with empirical calculation methods for wind-driven rain in the UK.

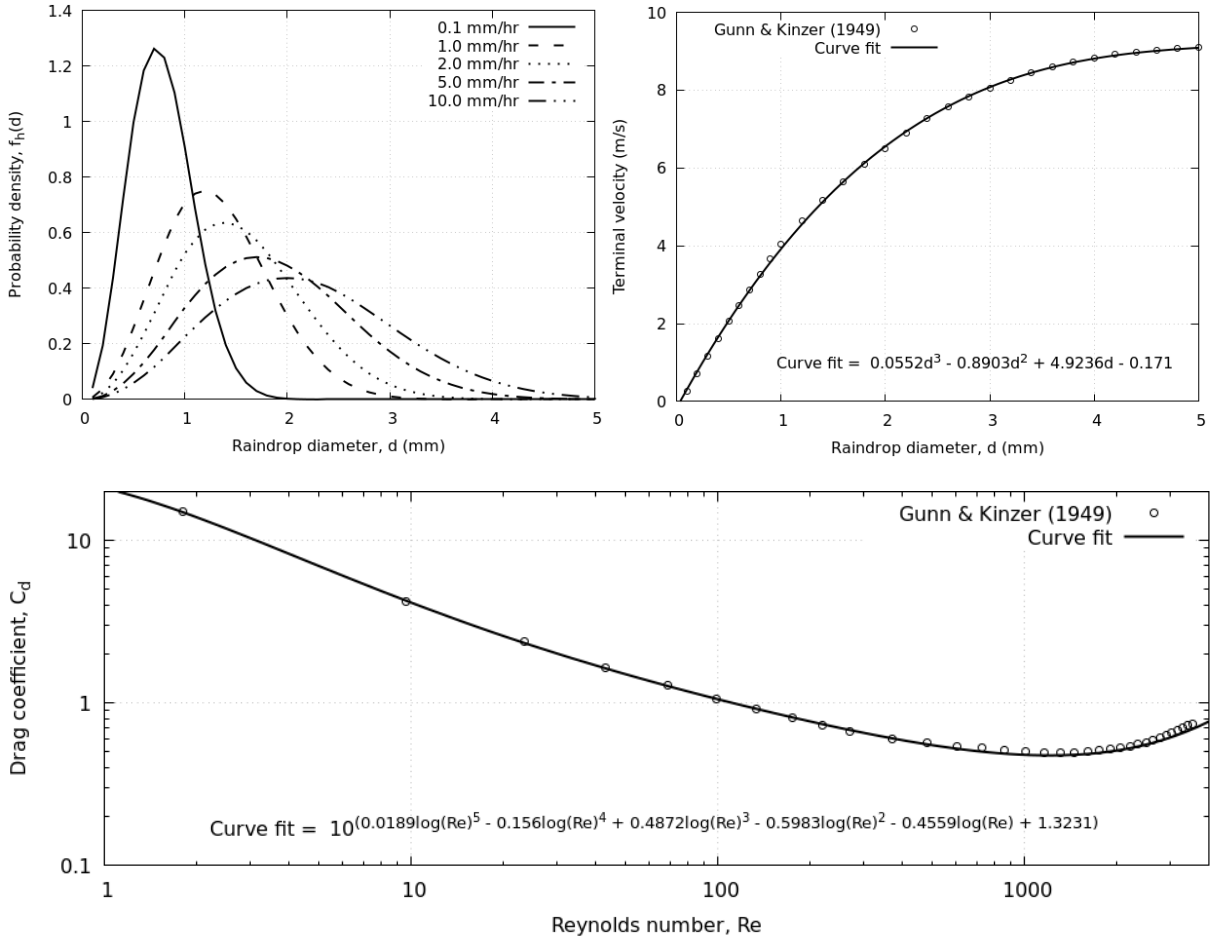

Figure 2: Raindrop size distribution (Best, 1950), terminal velocity and drag coefficient

3. Environmental Conditions

While rainfall intensity is usually defined in mm/hr it can vary over much shorter time periods. In Australia rain data is typically recorded at Bureau of Meteorology (BoM) automatic weather stations and reported in millimeters for given observation periods. While hourly BoM data is naturally equivalent to mm/hr this often yields an erroneously low rainfall intensity as rain events are often discontinuous across the hour. Very small sampling periods may also give unrealistic results if the rainfall depth gauge cannot register a reading during low intensity events. A more realistic rainfall intensity is obtained by using 5-minute BoM recordings. Multiplying by twelve converts the 5-min durations into continuous hourly equivalent rainfall intensity. Simultaneous average wind speed and direction recordings are also available.

In the following discussion the 5-min dataset from Melbourne Airport between October 19th 1997 and September 19th 2017 has been used. The dataset is first cleaned to remove invalid recordings and the percentage of non-zero rainfall recordings calculated, in this case 1.31% = 114 hrs/yr. It should be emphasized that 114 hrs/yr represents a set of 1368 5-min duration rainfall events occurring over a year rather than the number of hours per year in which any rain may occur. For Melbourne airport the maximum rainfall intensity is 129.6mm/hr (equivalent hourly intensity based on 5-min duration) with 50th percentile of 2.4mm/hr and 95th percentile at 9.6mm/hr, corresponding to classification of light and heavy rain, respectively (refer Table 1 below).

Table 1: Rainfall intensity classifications, AMS (2012)

Classification	Rainfall intensity (mm/hr)
Light	< 2.6
Medium	2.6 to 7.6
Heavy	> 7.6

A statistical analysis of wind during non-zero rainfall events is then undertaken. An example wind-rose during rain events for Melbourne Airport is shown in Figure 3. Given the complex interaction between raindrop diameters, trajectories and wind speed, an appropriate return period is difficult to define. Lawson (2001) discusses rainfall probability of occurrence and the expected angle of rainfall incidence for the UK, however application to numerical simulation of Australian conditions is not immediately obvious.

In the current paper, typical wind-driven rain conditions are defined as the 50th percentile rain intensity combined with the 50th percentile wind speed recorded during rain events. For worst-case wind-driven rain conditions the 95th percentile wind speed (occurring during rain events) are identified as a reasonable worst-case wind; however, since smaller drops are more easily driven by winds and the distribution of raindrop diameters skews towards smaller drops for lower intensity events, the worst-case wind-driven rain conditions were defined as 95th percentile wind speed with 50th percentile rainfall intensity. While the above definition of worst-case does not include extreme weather events where heavy rainfall is accompanied by very strong winds, it is argued these statistical definitions represent relevant wind-driven rain conditions for building design purposes.

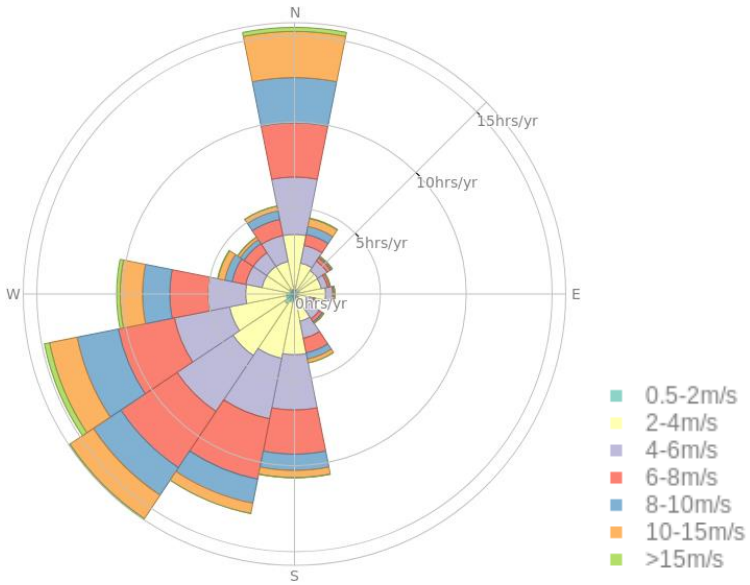

Figure 3: Wind rose during rain events at Melbourne Airport between 1997 and 2017

4. Numerical Modelling

The steady Atmospheric Boundary Layer (ABL) numerical model used in this work is documented in Jones et. al. (2017, 2018). Comparison between the simulated wind speed and turbulence intensity with the AS1170.2 (Standards Australia, 2011) shows less than 10% difference in both mean velocity and turbulence intensity is maintained through an empty domain.

A basic overview of the multiphase Euler method is given below. The governing equations for each rain phase are described by the mass and momentum equations,

$$\frac{\partial \alpha_k}{\partial t} + \nabla \alpha_k \boldsymbol{u}_{r_k} = 0 \tag{2}$$

$$\frac{\partial \alpha_k \boldsymbol{u}_{r_k}}{\partial t} + \nabla\left(\alpha_k \boldsymbol{u}_{r_k} \cdot \boldsymbol{u}_{r_k}\right) = \alpha_k g + \alpha_k \frac{3\mu_a}{\rho_r d^2} \frac{C_d Re_r}{4}\left(\boldsymbol{u}_a - \boldsymbol{u}_{r_k}\right) \tag{3}$$

where α_k and $\boldsymbol{u}_{r_k}$ are the phase fraction and velocity for the k[th] phase of rain, g is gravitational acceleration, ρ_r is the rain water density, μ_a is the dynamic air viscosity and C_d is droplet drag coefficient. Note the two sources of rain momentum are gravitational acceleration (first term on right-hand side of Eqn. 3) and raindrop drag forces (second term on RHS of Eqn. 3).

By splitting the rain phase velocity vector into mean and fluctuating components the usual Reynolds averaging process can be followed and Reynolds stress closure achieved with a rain phase Boussinesq eddy viscosity. The rain eddy viscosity can be related to the air turbulent viscosity using the Melville & Bray (1979) response (relaxation time) scales as a function of raindrop diameter and aerodynamic properties. A full derivation and description of this technique is given by Kubilay (2015).

Rain phase boundary conditions require definition of phase velocity and volume fraction. In the far-field raindrops are assumed to undisturbed by buildings and terrain. The vertical velocity is set to the raindrop terminal velocity and the horizontal velocity set equal to the local wind speed so that the relative rain speed is simply the terminal velocity. The volumetric ratio for phase k at the free-field boundaries is set to

$$\alpha_k = \frac{R_h f_h(R_h,d)}{V_t(d)} \tag{4}$$

Where V_t is terminal velocity, R_h is the horizontal rainfall intensity and f_h is the probability density of raindrop size from Best (1950) as illustrated in Figure 2.

Specific catch ratio (for each raindrop diameter) on a wall can simply be calculated as a ratio of the local phase fraction to the far-field phase fraction,

$$\eta_d(k) = \frac{R_{wdr}(k)}{R_h(k)} = \frac{\alpha_k |V_n(k)|}{R_h f_h(k)} \tag{5}$$

where V_n is the phase velocity normal to the wall. By multiplying the specific catch ratio by the probability density and integrating over all raindrops the GCR is recovered,

$$\eta = \int_d f_h(R_h,d)\eta_d \mathrm{d}d \tag{6}$$

5. WDR Intrusion

Wind is simulated from 16 cardinal directions following the methods in Jones et. al. (2017, 2018) with ABL reference velocity of 10m/s at 10m reference height. To simulate typical WDR conditions the velocity, turbulent viscosity, turbulent kinetic energy and dissipation are scaled from 10m/s to the 50[th] percentile wind speed for each direction described in Section 3. Using these frozen wind fields, a WDR simulation is conducted with 50[th] percentile rainfall intensity for each direction and the SCR and GCR calculated on each wall. A composite of typical rain intrusion patterns for all directions (η_{total}) is then created by multiplying the GCR for each wind direction ($\eta(\theta)$) by the probability of rain occurrence in that direction ($A(\theta)$) and summing over all directions,

$$\eta_{total} = \int_{\theta=0}^{360} A(\theta)\min(\eta(\theta),1)\mathrm{d}\theta \tag{7}$$

Note for the purposes of rain intrusion the GCR is limited to 1 in Equation 7 so that high rainfall intensity does not artificially skew results for low probability directions. This procedure is repeated for the 95[th]

percentile wind speed for each direction to obtain worst-case overall rain intrusion pattern. The typical and worst-case rain intrusion fields (η_{total}) are then plotted as contours across the occupied spaces.

6. Conclusions

This paper briefly reviewed properties of rainfall events and raindrop aerodynamics. A commercially viable design tool was then outlined based on the multiphase Euler method of Kubilay et. al. (2013, 2015). Statistical definitions were given for typical and worst-case wind-driven rain conditions. A rain intrusion post-processing algorithm was proposed that provides an easily understood visual representation of rain intrusion for typical and worst-case rain intrusion conditions.

References

Best, A.C., (1950), The Size Distribution of Raindrops. *Q. J. R. Met. Soc.* 76:16-36

Blocken, B. and Carmeliet, J., (2004), A Review of Wind-Driven Rain Research in Building Science. *J. Wind Eng. & Ind. Aero.* 92:1079-1130

Choi, E.C.C., (1993), Simulation of Wind-Driven-Rain Around a Building. *J. Wind Eng. & Ind. Aero.* 46-47:721-729

Gunn, R. and Kinzer, G., (1949), The Terminal Velocity of Fall for Water Droplets in Stagnant Air. *J. Met.* 6:234-8

Kubilay, A., Derome, D., Blocken, B. and Carmeliet, J., (2013), CFD Simulation and Validation of Wind-Driven Rain on a Building Façade with an Eulerian Multiphase Model. *Building and Environment* 61:69-81

Kubilay, A., Derome, D., Blocken, B. and Carmeliet, J., (2015), Numerical Modeling of Turbulent Dispersion for Wind-Driven Rain on Building Facades. *Environ. Fluid Mech.* 15:109-133

Jones, R., Mackenzie, N. and Moyle, T., (2017), Wind-Induced Human Comfort: Outline of a Computational Procedure. *9th Asia-Pacific Conference on Wind Engineering*, Dec 3-7, Auckland, New Zealand.

Jones, R., Mackenzie, N. and Moyle, T., (2018), Guidelines for Practical Application of CFD to Pedestrian Wind Environment in Australasia. *19th AWES Workshop*, April 4-6, Torquay, Victoria

Lawson, T. (2001), Building Aerodynamics. *Imperial College Press*, London

Melville, W. and Bray, K., (1979), A Model of the Two-Phase Turbulent Jet. *Int. J. Heat Mass Transf.* 22:647-656

Standards Australia, (2011), Structural Design Actions Part 2: Wind Actions. AS/NZS 1170.2:2011